Monthly Notices
of the
ROYAL ASTRONOMICAL SOCIETY

MNRAS **507,** 43–54 (2021)
Advance Access publication 2021 July 15

https://doi.org/10.1093/mnras/stab2012

The GALAH survey: accreted stars also inhabit the Spite plateau

Jeffrey D. Simpson [1,2]★ Sarah L. Martell [1,2] Sven Buder [2,3] Joss Bland-Hawthorn [2,4] Andrew R. Casey [2,5] Gayandhi M. De Silva,[6,7] Valentina D'Orazi,[8] Ken C. Freeman,[2,3] Michael Hayden,[2,4] Janez Kos,[9] Geraint F. Lewis [4] Karin Lind,[10] Katharine J. Schlesinger,[3] Sanjib Sharma [2,4] Dennis Stello,[1,2,4] Daniel B. Zucker,[2,7,11] Tomaž Zwitter [9] Martin Asplund,[12] Gary Da Costa [2,3] Klemen Čotar,[9] Thor Tepper-García,[2,4,13] Jonathan Horner [14] Thomas Nordlander [2,3] Yuan-Sen Ting,[3,15,16,17] and Rosemary F. G. Wyse [18]
(The GALAH Collaboration)

Affiliations are listed at the end of the paper

Accepted 2021 July 5. Received 2021 July 4; in original form 2021 May 23

ABSTRACT

The European Space Agency (ESA) *Gaia* mission has enabled the remarkable discovery that a large fraction of the stars near the solar neighbourhood are debris from a single in-falling system, the so-called *Gaia*-Sausage-Enceladus (GSE). This discovery provides astronomers for the first time with a large cohort of easily observable, unevolved stars that formed in a single extragalactic environment. Here we use these stars to investigate the 'Spite plateau' – the near-constant lithium abundance observed in unevolved metal-poor stars across a wide range of metallicities ($-3 <$ [Fe/H] < -1). Our aim is to test whether individual galaxies could have different Spite plateaus – e.g. the interstellar medium could be more depleted in lithium in a lower galactic mass system due to it having a smaller reservoir of gas. We identified 93 GSE dwarf stars observed and analysed by the GALactic Archaeology with HERMES (GALAH) survey as part of its Data Release 3 (DR3). Orbital actions were used to select samples of GSE stars, and comparison samples of halo and disc stars. We find that the GSE stars show the same lithium abundance as other likely accreted stars and *in situ* Milky Way stars. Formation environment leaves no imprint on lithium abundances. This result fits within the growing consensus that the Spite plateau, and more generally the 'cosmological lithium problem' – the observed discrepancy between the amount of lithium in warm, metal-poor dwarf stars in our Galaxy, and the amount of lithium predicted to have been produced by big bang nucleosynthesis – is the result of lithium depletion processes within stars.

Key words: stars: abundances – Galaxy: evolution – Galaxy: halo.

1 INTRODUCTION

^{7}Li is one of the four stable nuclides (along with ^{2}H, ^{3}He, and ^{4}He) that are predicted by big bang nucleosynthesis (BBN) to have been synthesized during the first minutes of the Universe (a theory first proposed by Alpher, Bethe & Gamow 1948, see recent reviews of BBN from Cyburt et al. 2016; Fields et al. 2020). In the standard model of BBN, the amounts of these primordial abundances formed are strongly dependent on the baryon-to-photon ratio, which can be estimated from the cosmic microwave background. Observations in astrophysical environments have measured abundances that are in agreement with BBN predictions (Fields et al. 2020), i.e. ^{2}H from quasar spectra (e.g. Cooke, Pettini & Steidel 2018), ^{4}He from metal-poor extragalactic H II regions (e.g. Aver, Olive & Skillman 2015), ^{7}Li in low-metallicity gas in the Small Magellanic Cloud (Howk et al. 2012) – though the latter is dependent on the chemical evolution model.

There has long been tension between the BBN-predicted primordial abundance of ^{7}Li and the abundance measured in warm, metal-poor dwarf stars of our Galaxy. These stars have thin convective layers, and models predict they formed from gas that had a (near-) primordial Li abundance, and they will retain this formation Li abundance in their photosphere (Deliyannis, Demarque & Kawaler 1990). As first identified by Spite & Spite (1982a,b), and subsequently confirmed (e.g. Bonifacio & Molaro 1997; Ryan, Norris & Beers 1999; Asplund et al. 2006; Meléndez et al. 2010; Sbordone et al. 2010), across a large range of metallicity ($-3 <$ [Fe/H] < -1) these stars do have a near-constant Li abundance creating the so-called 'Spite plateau'. But, the Spite plateau abundance is 3–4 times lower than ^{7}Li abundance predicted by BBN. This discrepancy is known as the 'cosmological lithium problem' (see the review by Fields 2011).

The concordance of the predictions from BBN and the observed abundances for the ^{2}H, ^{3}He, and ^{4}He nuclides means that it is not BBN at fault. There is a growing consensus that the Li depletion in these stars is from extra mixing below the convection zone due to rotation (e.g. Deliyannis et al. 1990; Pinsonneault, Deliyannis & Demarque 1992), diffusion and turbulent mixing (e.g. Michaud &

★ E-mail: jeffrey.simpson@unsw.edu.au

Charbonneau 1991; Richard 2012), and internal gravity waves (e.g. Charbonnel & Talon 2005).

In this work, we investigate an alternative hypothesis to explain the Spite plateau: that observable metal-poor dwarf stars simply did not form with a near-primordial lithium abundance. The Spite plateau could be the result of pre-processing of interstellar medium through previous generations of stars, as proposed by e.g. Piau et al. (2006). This raises the question that we wish to answer: *Does the stellar formation environment affect the Spite plateau?*

Unfortunately, it is not practical to measure the lithium abundance of dwarf stars in external galaxies with the current suite of telescopes.[1] Fortunately, it is thought that a sizeable fraction of the Galactic halo stars were accreted (e.g. Ibata, Gilmore & Irwin 1994; Helmi et al. 1999; Ibata et al. 2004; Abadi et al. 2010; Starkenburg et al. 2017, and reviews by Bland-Hawthorn & Gerhard 2016; Helmi 2020), with the accepted paradigm for the growth of galaxies like our Milky Way featuring the hierarchical mergers of large galaxies with smaller dwarf galaxies (e.g. Searle & Zinn 1978; White & Frenk 1991; Cole et al. 2002; Venn et al. 2004; Oser et al. 2010). These dwarf galaxies are completely disrupted and are mixed throughout the Galactic halo.

Until recently, globular clusters provided the only dwarf stars that could be easily identifiable as being born *ex situ* that are observationally accessible. For instance, dwarf stars in ω Cen show lithium abundances consistent with field stars (Monaco et al. 2018). Using models of diffusion to estimate their initial abundances, Mucciarelli et al. (2014) observed giant stars in M54, finding the Galactic Spite plateau value. We do note two complications with globular clusters: first, the question of which globulars are accreted and which formed *in situ* is an active area of research (e.g. Forbes & Bridges 2010; Massari, Koppelman & Helmi 2019; Horta et al. 2020; Keller et al. 2020); and secondly, the observations that the first and second generations of stars have the same lithium abundances, despite the latter stars forming from material processed through the former (see discussion in the review by Gratton 2020).

Now, thanks to the combination of deep photometric surveys and the data contained in the Second Data Release of the European Space Agency (ESA) *Gaia* mission (Gaia Collaboration et al. 2016, 2018), it has been shown that the halo of the Galaxy contains spatial and kinematic substructure – the identifiable remnants of past accretion events (Ibata et al. 2018; Malhan, Ibata & Martin 2018; Yan et al. 2018; Barbá et al. 2019; Myeong et al. 2019; Borsato, Martell & Simpson 2020; Naidu et al. 2020; Yuan et al. 2020, and see the review by Helmi 2020). Some stars of the >50 known 'stellar streams' (see Mateu, Read & Kawata 2018, and references therein) have been spectroscopically observed (e.g. Ibata, Malhan & Martin 2019; Li, Wang & Milone 2019; Ji et al. 2020; Li et al. 2020; Simpson et al. 2020). For the S2 stream, the likely result of a disrupted dwarf galaxy, Aguado et al. (2021) measured the lithium abundance for a handful of dwarf stars and found the lithium behaviour to be like that of the rest of the halo.

On a larger scale, a significant proportion of the halo stars near the Sun appear to have been accreted from a single dwarf galaxy (e.g. Nissen & Schuster 2010; Belokurov et al. 2018; Haywood et al. 2018; Helmi et al. 2018; Myeong et al. 2018a,b; Fattahi et al. 2019; Naidu et al. 2020). *Gaia*-Sausage-Enceladus (GSE) presents the exciting prospect of a large number of main-sequence stars from a single dwarf galaxy that can be readily observed with current ground-based telescopes. These stars have a relatively unique kinematic signature – eccentric orbits with low angular momenta – making them easy to distinguish from other halo stars. For moderately metal-poor members ([Fe/H] ≥ -1.3) they can also be chemically tagged as coming from the GSE due to their low [α/Fe] compared to *in situ* stars (Nissen & Schuster 2010; Helmi et al. 2018; Monty et al. 2020).

Previous studies have looked at lithium in the GSE stars. Nissen & Schuster (2012) measured the lithium abundances of 25 stars in their low-α halo sequence – which we now know to be GSE – finding no significant systematic difference in the lithium abundances of high- and low-α stars. Molaro, Cescutti & Fu (2020) and Cescutti, Molaro & Fu (2020) both looked at lithium in 39 GSE stars using abundances from literature compilations. They found that the Spite plateau in GSE to be the same as in the rest of the Milky Way.

In this work, we expand upon those results, presenting the lithium abundance of 93 GSE dwarf stars serendipitously observed and homogeneously analysed as part of the Third Data Release (Buder et al. 2021) of the GALactic Archaeology with HERMES survey (GALAH; De Silva et al. 2015). GALAH is a massive spectroscopic survey of the local Galactic volume, and we explore whether the lithium abundances of GSE stars are consistent with the abundances of other Galactic populations with likely *in situ* and *ex situ* origins. We test the hypothesis that the Spite plateau is not the result of galactic chemical evolution.

This work is structured as follows. Section 2 describes the observation, reduction, and analysis. Section 3 considers how lithium abundances change with stellar properties. Section 4 explains how the GSE stars were selected. Section 5 compares and contrasts the Spite plateau for various subsamples of Milky Way stars. Section 6 comments on a handful of very Li-rich metal-poor stars. Section 7 summarizes the paper.

2 OBSERVATION, REDUCTION, AND ANALYSIS

The spectroscopic data used in this work come from the 588 571 stars of the Data Release 3 (DR3) of the GALAH survey (Buder et al. 2021) – the combination of GALAH survey (De Silva et al. 2015; Martell et al. 2017; Buder et al. 2018), the *K2*-HERMES survey (Wittenmyer et al. 2018; Sharma et al. 2019), and the *TESS*-HERMES survey (Sharma et al. 2018). All observations used the HERMES spectrograph (Sheinis et al. 2015) and the 2-degree Field (2dF) fibre positioning system (Lewis et al. 2002) at the 3.9-m Anglo-Australian Telescope. HERMES records ~1000 Å of the optical spectrum at a spectral resolution of $R \approx 28\,000$ across four non-contiguous sections, which includes the neutral Li resonance lines at 6708 Å. The spectra were reduced with a custom IRAF pipeline (Kos et al. 2017).

All stellar parameter and abundance values in this work are from Buder et al. (2021), with the lithium abundance for each star determined from synthesis of the 6708 Å Li line and includes non-local thermodynamic equilibrium (LTE) corrections. In this work, we use the form $A_{\rm Li} = \log[n_{\rm Li}/n_{\rm H}] + 12$, where $n_{\rm Li}$ and $n_{\rm H}$ are the number densities of lithium and hydrogen, respectively. On this scale, the BBN prediction is $A_{\rm Li} = 2.75 \pm 0.02$ (Pitrou et al. 2018). Examples of HERMES spectra of dwarf stars for the region around 6708 Å are shown in Fig. 1. Qualitatively, these spectra confirm the

[1] In the future it will be possible, e.g. GMT-Consortium Large Earth Finder (G-CLEF) on the Giant Magellan Telescope will be able to acquire in 1.5 h $R \approx 23\,000$ spectra of signal-to-noise ratio ~10 for the brightest turn-off stars in the Large Magellanic Cloud.

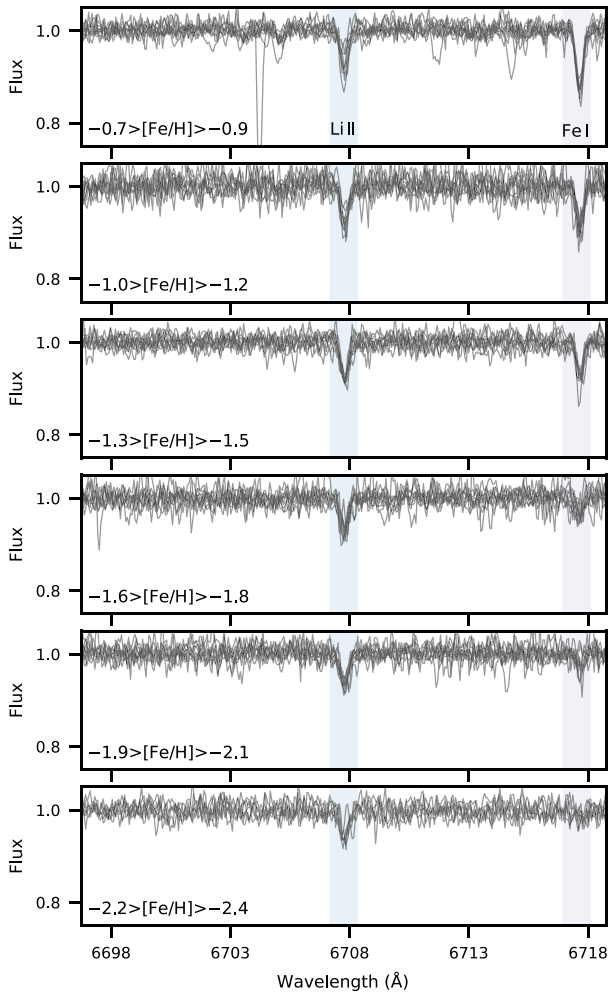

Figure 1. Pseudo-continuum normalized HERMES spectra for the Li 6708 Å region (shaded blue band). In each panel there are up to 10 randomly chosen stars in a narrow [Fe/H] range (as indicated on each panel) from a representative region of the $T_{\rm eff}$–log g space for dwarf stars ($5975 < T_{\rm eff} < 6175$ K and $4.0 < \log g < 4.4$). The purple shaded band is the Fe 6718 Å line seen to weaken with decreasing metallicity. There is little variation in the strength of the lithium line in a given metallicity bin, qualitatively confirming the presence of the Spite plateau.

existence of the Spite plateau – i.e. at a given [Fe/H] and $T_{\rm eff}$ there is little variation in the strength of the lithium line.

We apply data quality selections to identify a sample of dwarf stars (defined as surface gravity $\log g > 3.65$ and absolute G magnitude >1.5) with reliable stellar parameters and abundances. For each star we require: (i) GALAH DR3 flag `flag_sp` $= 0$ and `flag_fe_h` $= 0$ (no problems noted in the input data, reduction, analysis, or iron abundance determination); (ii) a five-parameter solution from *Gaia* Early Data Release 3 (EDR3; Gaia Collaboration et al. 2021) to allow for orbital calculations; (iii) the red camera spectrum (which contains the Li line) signal-to-noise ratio >30 pixel^{-1}. These selections identify the set of 197 921 dwarf stars that we consider for the remainder of this work. When we are considering the abundance of element `x`, we also require that the GALAH flag `flag_x_fe` $= 0$ (no problems noted in the abundance determination). For instance, of the 197 921 dwarf stars, 86 320 dwarf stars with reliable lithium abundances.

The Galactic orbital properties of each star are taken from Buder et al. (2021). Briefly, this used GALPY (Bovy 2015) with values from GALAH DR3 and *Gaia* EDR3, McMillan2017 potential (McMillan 2017) and the values $R_{\rm GC} = 8.21$ kpc and $v_{\rm circular} = 233.1\,{\rm km\,s^{-1}}$ (Gravity Collaboration et al. 2019). It set $(U, V, W)_{\odot} = (11.1, 15.17, 7.25)\,{\rm km\,s^{-1}}$ in keeping with Reid & Brunthaler (2004) and Schönrich, Binney & Dehnen (2010). Distances are primarily from the GALAH DR3 age and mass value-added catalogue, which mostly incorporated distances found by the Bayesian Stellar Parameters estimator (BSTEP; described in Sharma et al. 2018).

3 EFFECTS OF STELLAR PROPERTIES ON LITHIUM ABUNDANCES

Lithium is a fragile element in stars. Along with Be and B (see the review of Randich & Magrini 2021) it is easily destroyed in stellar interiors at a relatively low temperature (2.6×10^6 K for Li; Gamow & Landau 1933; Salpeter 1955). This destruction is observed in the Sun: the solar photospheric lithium abundance is $A_{\rm Li} = 1.05 \pm 0.01$, while the meteoritic lithium abundance is 3.26 ± 0.05 (Asplund et al. 2009). Li burning will occur in stars whenever there is the ability to transport surface material to the hotter interior. There are various stellar atmospheric processes – the convective zone, atomic diffusion (e.g. Michaud & Charbonneau 1991; Richard 2012), rotation-induced mixing (e.g. Deliyannis et al. 1990; Pinsonneault et al. 1992), and internal gravity waves (e.g. Charbonnel & Talon 2005) – competing to both drive and inhibit this mixing. The dominant mechanism depends on the mass, metallicity, and evolutionary stage of the star. For this work it is necessary to identify stars that are the least affected by Li depletion, and therefore their current Li abundance is most representative of their birth abundance.

Fig. 2 shows the 86 320 dwarf stars from our sample with reliable lithium abundance (e.g.) in the $T_{\rm eff}$–log g plane, and their $A_{\rm Li}$ with respect to $T_{\rm eff}$, log g, [Fe/H], and signal-to-noise in the HERMES spectra. The coolest stars, with the highest and lowest log g in the sample, likely experienced a large amount of surface lithium depletion and form 'tails' of low $A_{\rm Li}$ in Fig. 2(c). The hottest stars retain most of their formation lithium because they have thin convective zones and are nearly unaffected by either rotation-induced mixing or diffusion. Seen in Fig. 2(a) as the 'warm peninsula', these stars also form the overdensity of roughly solar metallicity stars with $A_{\rm Li} \sim 3$ in Fig. 2(d). Meanwhile for stars in the range $6400 < T_{\rm eff} < 6850$ K, rotation-induced mixing is the dominant mechanism, causing severe lithium destruction and the so-called 'lithium dip' (a feature first observed in open clusters; e.g. Wallerstein, Herbig & Conti 1965; Boesgaard et al. 2016). This Li dip manifests as the region of the $T_{\rm eff}$–log g diagram lacking in almost any stars with reliable lithium measurements. The Li dip and 'warm peninsula' are explored in detail using GALAH data by Gao et al. (2020).

For investigating the Spite plateau, as has been done previously in the literature (e.g. Meléndez et al. 2010), we want to identify a stellar parameter selection that includes only those stars hot enough to inhibit significant Li depletion, whilst simultaneously maximizing our sample size of metal-poor stars. Experimentation identified a temperature cut-off of $T_{\rm eff} > 5850$ K as the best compromise between selecting those stars least affected by Li depletion, and retaining a large sample of stars. In Fig. 2, we highlight stars with [Fe/H] < -0.8 (i.e. the metallicity range of halo stars): black dots for stars with $T_{\rm eff} > 5850$ K, and fuchsia crosses for stars below this

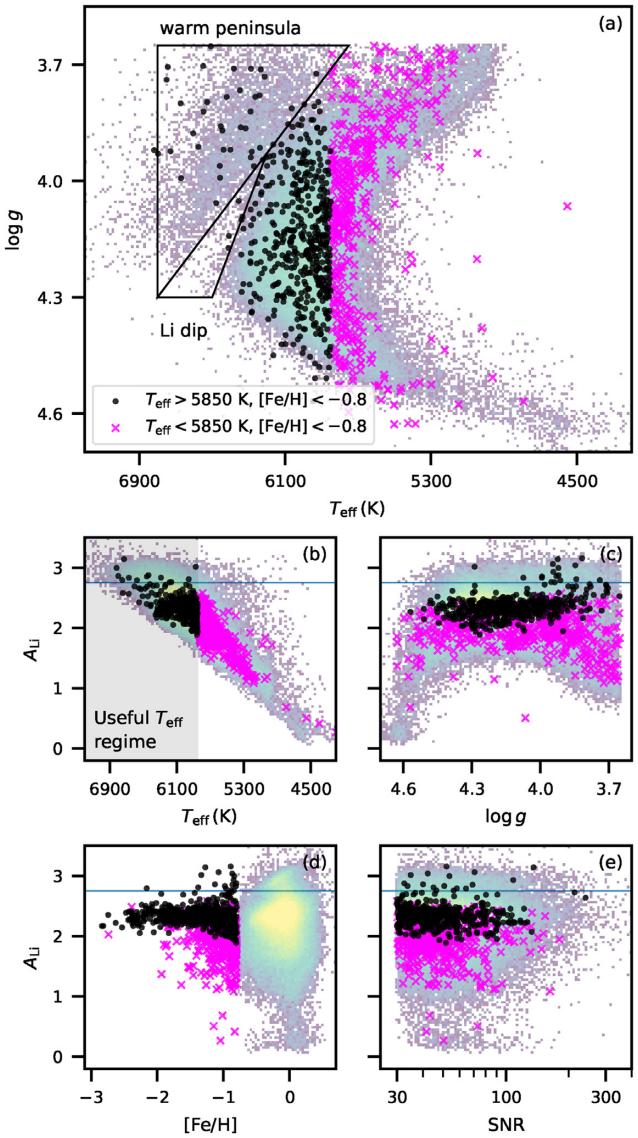

Figure 2. The distribution of the 86 320 GALAH stars with reliable lithium abundances (i.e. `flag_li_fe` = 0) in (a) $T_{\rm eff}$–log g; and $A_{\rm Li}$ versus (b) $T_{\rm eff}$, (c) log g, (d) [Fe/H], and (e) signal-to-noise ratio (SNR). The horizontal blue line is the big bang nucleosynthesis (BBN) lithium abundance ($A_{\rm Li} = 2.75 \pm 0.02$; Pitrou et al. 2018). Highlighted are all stars with [Fe/H] < -0.8, with black dots for stars with $T_{\rm eff} > 5850$ K, and fuchsia crosses for stars with $T_{\rm eff} < 5850$ K. The hotter stars are our selection of metal-poor stars that are least affected by lithium depletion on the main sequence. The cooler stars might otherwise have been thought to form part of the Spite plateau, but can be seen to have much lower lithium abundances. As this figure only shows stars with reliable lithium abundances, the morphology of the $T_{\rm eff}$–log g plane shows two interesting features, highlighted with triangular regions in panel (a): the 'warm peninsula' of Li-rich dwarf stars, and the 'Li dip' where there is a dearth of stars with lithium measurements.

temperature. There are a handful of hotter metal-poor stars that fall on to the Li-rich 'warm peninsula' – the stars least affected by any Li depletion. However, as we will see in Section 5, none of these stars are found in our halo samples. Of the 86 320 dwarf stars with reliable Li abundances in our data set, 53 761 have $T_{\rm eff} > 5850$ K. For the 992 dwarf stars with metallicity [Fe/H] < -0.8, 485 dwarf stars have $T_{\rm eff} > 5850$ K.

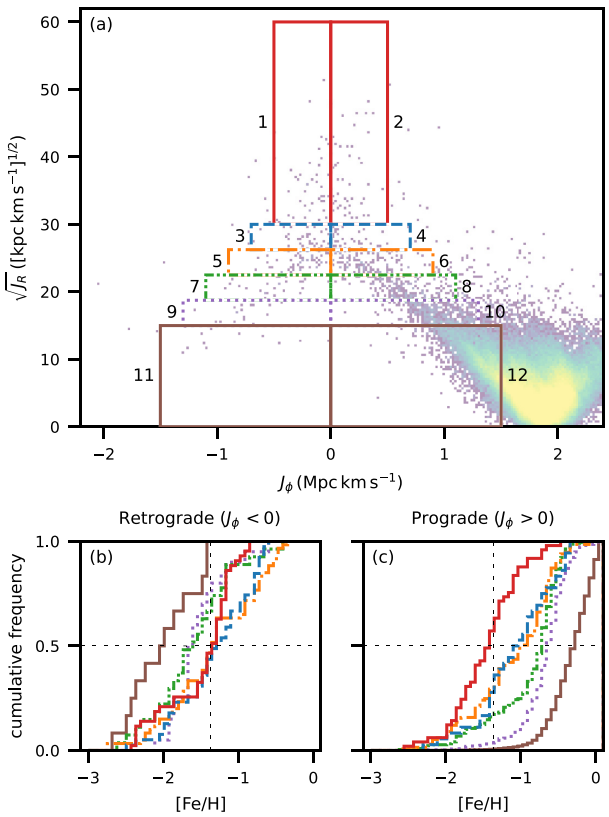

Figure 3. The cumulative metallicity distribution functions (CDFs) for bins of stars in J_ϕ–$\sqrt{J_R}$ action space. Panel (a) shows the log-density number distribution of all GALAH DR3 dwarf stars in J_ϕ–$\sqrt{J_R}$ action space, along with the location of the bins used for each CDF. Panels (b) and (c) show, respectively, the CDF for the retrograde (odd-numbered bins; $J_\phi < 0$) and prograde (even-numbered bins; $J_\phi > 0$). The vertical dashed lines in panels (b) and (c) mark the median metallicity of the combination of all stars in bins 1 and 2 ([Fe/H] $= -1.37$). The horizontal line is for the 50th percentile of the CDF. The CDF for bins 1 and 2 (red on all panels) is the most consistent of all the pairings of prograde and retrograde bins; these bins form our selection of GSE stars.

4 *GAIA*-SAUSAGE-ENCELADUS MEMBER SELECTION

One of the major discoveries facilitated by *Gaia* is that about half of the metal-poor stars in the local halo appear to have been accreted from single dwarf galaxy called *Gaia*-Sausage-Enceladus (GSE; Belokurov et al. 2018; Haywood et al. 2018; Helmi et al. 2018; Myeong et al. 2018b). Here, we identify likely accreted GSE stars using the same method as Feuillet et al. (2020), who cleanly selected GSE members as those with Galactic orbits that had angular momentum $J_\phi \sim 0$ and large radial action J_R.

Fig. 3 is similar to fig. 5 from Feuillet et al. (2020), but for our sample of 197 921 GALAH DR3 dwarfs. The J_ϕ–$\sqrt{J_R}$ space is divided into pairs of prograde ($J_\phi > 0$) and retrograde ($J_\phi < 0$) bins for a range of $\sqrt{J_R}$. As Feuillet et al. (2020) noted, stars with $\sqrt{J_R} > 30\,({\rm kpc\,km\,s^{-1}})^{1/2}$ (i.e. our bins 1 and 2, which will form our GSE selection) have similar cumulative metallicity density function (CDF) for both the prograde and retrograde bins – consistent with them having a single origin. Meanwhile, in all bins other than 1 and 2 ($\sqrt{J_R} < 30\,({\rm kpc\,km\,s^{-1}})^{1/2}$), each pairing of the prograde and retrograde bins shows different CDFs. All of the prograde bins are

more metal rich than bins 1 and 2, due to the formers' inclusion of more disc-like (and therefore more metal rich) stars. The combined sample of stars from bins 1 and 2 has a median metallicity of [Fe/H] = −1.37, which is marked with dashed vertical lines in Figs 3(b) and (c). This is more metal poor than the median metallicity of [Fe/H] = −1.17 found by Feuillet et al. (2020) for the same kinematic selection, but their sample was giants with photometric metallicity estimates.

We combine bins 1 and 2 to be the selection of GSE stars and highlight those stars in a variety of observational spaces in Fig. 4. Three additional groups of stars are identified for comparison to our GSE sample, and these regions are indicated in Fig. 4(a). The details of these selections are as follows:

(i) 93 GSE stars: $(-0.5 < J_\phi < 0.5)\,\mathrm{Mpc\,km\,s^{-1}}$ and $\sqrt{J_R} > 30\,(\mathrm{kpc\,km\,s^{-1}})^{1/2}$;
(ii) 102 retrograde orbiting halo stars: $J_\phi < 0\,\mathrm{Mpc\,km\,s^{-1}}$ and $\sqrt{J_R} < 25\,(\mathrm{kpc\,km\,s^{-1}})^{1/2}$;
(iii) 208 prograde orbiting stars that will be a mixture of halo and dynamically thick disc stars: $(0 < J_\phi < 1)\,\mathrm{Mpc\,km\,s^{-1}}$ and $20 < \sqrt{J_R} < 25\,(\mathrm{kpc\,km\,s^{-1}})^{1/2}$;
(iv) 196 619 disc stars, which are highly likely to have formed *in situ*: $J_\phi > 0.9\,\mathrm{Mpc\,km\,s^{-1}}$ and $\sqrt{J_R} < 15\,(\mathrm{kpc\,km\,s^{-1}})^{1/2}$.

Different authors have used different selections for identifying members of GSE. The J_R–J_ϕ selection used in this work has much overlap with these other selections, but has the advantage of having less contamination from non-GSE stars. Here we comment on the similarities and differences between the various selections used in other works.

(i) Belokurov et al. (2018) used the v_R versus v_ϕ plane to identify their 'Sausage' of stars at $v_\phi \sim 0\ \mathrm{km\,s^{-1}}$. Their selection includes stars at all v_R, rather than our selection that is limited to $|v_R| > \sim 200\ \mathrm{km\,s^{-1}}$ (Fig. 4e). Having a lower limit in J_R for GSE would result in stars with smaller $|v_R|$ being included, while maintaining the range of v_ϕ.
(ii) Koppelman, Helmi & Veljanoski (2018) and Helmi et al. (2018) identified their GSE stars as a 'plume' of stars in the J_ϕ–energy space (Fig. 4c) and in the Toomre diagram (Fig. 4f), which is where our GSE selection stars can also be found. The region used by Helmi et al. (2018) was more retrograde and includes stars that are found on the 'arm' of stars that extend to low $\sqrt{J_R}$ and negative J_ϕ region of Fig. 4(a) that we have defined as being the 'retrograde halo'.
(iii) Myeong et al. (2019) selected their GSE sample using the action space map (Fig. 4d). Their selection translates to a narrower range of angular momentum ($|J_\phi| \leq 0.1\,\mathrm{Mpc\,km\,s^{-1}}$), but like Belokurov et al. (2018), to a lower value of J_R than we have used.
(iv) Our selection of stars has identified stars along a narrow sequence in the colour–magnitude diagram (CMD; Fig. 4b) that is consistent with the blue sequence found by Haywood et al. (2018) and others.

4.1 Possible contamination of the sample

In this subsection, we consider if there is any contamination of our selection of GSE stars with non-member stars.

We have not used abundance information as a chemical tag of GSE stars (e.g. Mg, Mn, and Al as used by Das, Hawkins & Jofré 2020), as this would limit us to only the metal-rich stars, due to the limitations of HERMES spectra for metal-poor stars. In the metallicity range −2.5 < [Fe/H] < −2.0, there are 95 dwarf stars in GALAH DR3 with reliable parameters, of which 59 (62 per cent) have a reliable A_{Li}, but only 16 (17 per cent) have [α/Fe], 10 (11 per cent) have [Mg/Fe], 10 (11 per cent) have [Mn/Fe], and none have [Al/Fe].

It is still useful to consider the abundance for the metal-rich end of the GSE selection. Fig. 5 shows a comparison of the abundance distributions of A_{Li}, [α/Fe], [Mg/Fe], and [Na/Fe] for GSE (left-hand column) and the stars from the retrograde halo sample (right-hand column). α-elements like Mg and the odd-Z elements like Na have well-known 'knee' in the Tinsley–Wallerstein diagram (Buder et al. 2021) when Type Ia supernova (SN Ia) began to dominate Type II supernova (SN II) and decrease the abundance of some light elements in the interstellar medium (e.g. Kobayashi, Karakas & Lugaro 2020). For the Milky Way this is at [Fe/H] ∼ −1, while lower galactic mass systems have their knee at a lower metallicity (Venn et al. 2004). We confirm this previously observed feature of GSE (Helmi et al. 2018; Monty et al. 2020). We find only two GSE stars (marked with black crosses in Figs 4 and 5) that have [α/Fe] values clearly more consistent with the α-rich disc.

There is one further possible contaminant star. This star, marked with open black circle in Fig. 4, has a location on T_{eff}–log g diagrams and CMD (Figs 4b and h, respectively) that makes the star too young and/or massive to belong to GSE. Briefly, there are three possible explanations: (1) it has relatively large errors in its orbital parameters, so it could simply be the result of unreliable measurements; (2) it is a young *in situ* Milky Way star that has ended up in a halo orbits by some dynamical process (Famaey et al. 2005; Bensby et al. 2007; Williams et al. 2011; Casey et al. 2014); (3) it is a blue straggler (BS) star. BS stars are main-sequence-like stars that stand out in roughly coeval populations because they are significantly more massive than the normal main-sequence turn-off mass of the population (Bailyn 1995). Many globular clusters have a population of BS, and the leading mechanisms invoked to explain their presence are binary mergers and/or stellar collisions. Identifying them in the field is much more difficult because you are no longer considering a 'closed box' environment, but estimates suggest the fraction of the nearby halo BS is of the order of 20 per cent (Casagrande 2020).

Overall, there appears to be little obvious contamination of non-GSE stars into our sample. Neither the possible BS stars nor the α-rich stars affect the analysis of the Spite plateau as they, by chance, lack reliable lithium abundances.

5 THE LITHIUM PLATEAU AND ENRICHMENT IN GSE

Using the T_{eff} selection from Section 3 and the dynamical selections from Section 4, we now compare the properties of the Spite plateau for subpopulations of the Milky Way (the selected stars are listed in Table 1). As discussed in Section 1, the aim of this work is to explore the lithium abundances of GSE stars and compare them to the rest of the Milky Way halo (a mixture of accreted and *in situ* stars) and the Milky Way disc stars (likely *in situ* formation), to see if there is any difference that could be the result of formation environment.

Fig. 6 compares the four populations defined in Section 4: GSE (first column), the retrograde halo (second column), the prograde halo (third column), and the disc (fourth column). The top row shows the A_{Li} distribution with [Fe/H], with other rows showing for context the [Fe/H]–[α/Fe], J_ϕ–$\sqrt{J_R}$, and T_{eff}–log g distributions of the stars. For each population we only highlight the stars with $T_{\mathrm{eff}} > 5850$ K (Section 3); additionally for the rightmost column, the panels showing the disc stars, only those stars with [Fe/H] < −0.6 are shown for visual clarity (this metallicity was chosen as it is the observed metallicity ceiling of the other three samples). The purple

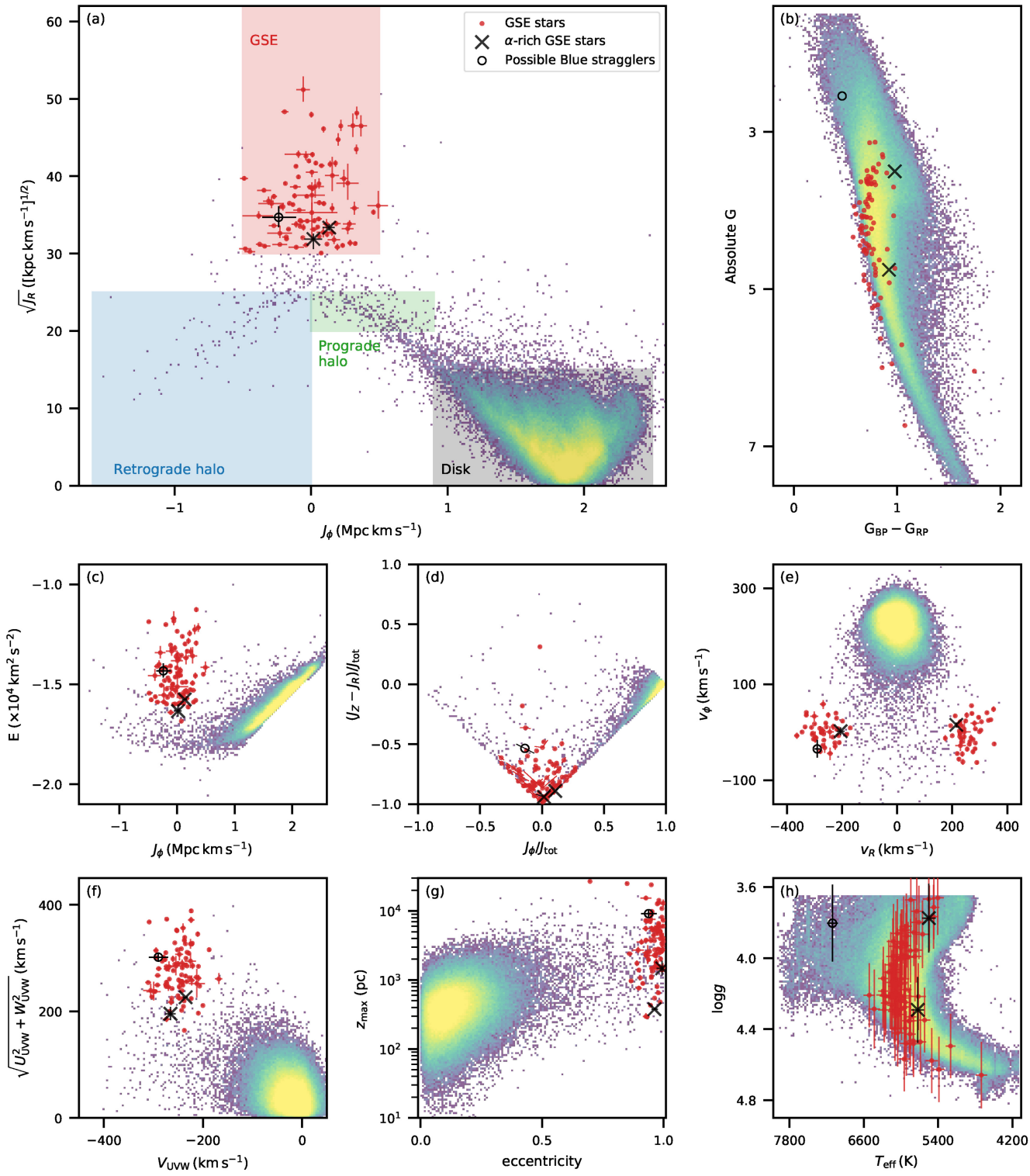

Figure 4. Distributions of all GALAH dwarfs in a variety of dynamical, orbital, and stellar parameter spaces that have been used to identify GSE stars: (a) the J_ϕ–$\sqrt{J_R}$ action-angle space; (b) the colour–(absolute) magnitude diagram (CMD); (c) J_ϕ and orbital energy; (d) J_ϕ and $(J_Z - J_R)$ normalized by $J_{tot}(= J_Z + J_R + |J_\phi|)$; (e) the Galactocentric velocity components v_r and v_ϕ; (f) the Toomre diagram; (g) orbital eccentricity and the largest distance travelled out of the Galactic plane z_{max}; and (h) T_{eff}–log g. In panel (a) the selections used to identify the various dynamical subsamples are shown, and the stars within the GSE box are highlighted in red in all panels, except for three GSE stars that are highlighted in black. These latter stars are either much hotter than all other stars (possibly blue straggler stars; black open circle symbols); or are α-rich stars (see Fig. 5; black crosses).

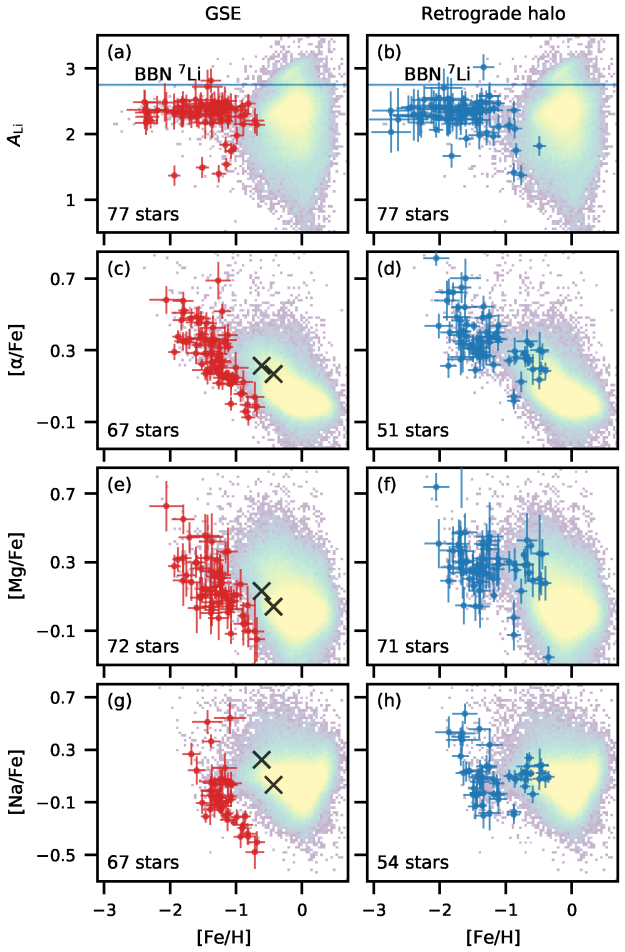

Figure 5. Abundance distributions for A_{Li}, [α/Fe], [Mg/Fe], and [Na/Fe] for the GSE stars (left-hand column; red dots with error bars) and retrograde halo sample (right-hand column; blue dots with error bars), compared to the full sample of dwarf stars used in this work (background log-density distribution). The black symbols are the same as in Fig. 4, indicating dynamically selected GSE stars that are either α-rich (crosses) or much hotter than all other GSE stars (unfilled circles). The blue horizontal lines in panels (a) and (b) indicate the BBN prediction for A_{Li} ($A_{Li} = 2.75 \pm 0.02$; Pitrou et al. 2018). For the other elements, comparing the GSE sample to the retrograde halo sample, for stars with [Fe/H] $> \sim -1$, the GSE stars are generally all lower in abundance, while the retrograde halo stars have abundances more consistent with the α-rich disc.

square symbols further highlight stars within each sample that have $A_{Li} > 2.65$ – stars that are near or above the BBN lithium abundance; these stars will be discussed in Section 6.

As could already be clearly seen in Figs 5(a) and (b), GALAH DR3 confirms the result from Molaro et al. (2020) and Cescutti et al. (2020) – GSE shows broadly the same Spite plateau lithium abundance as other stars in the Milky Way halo. Fig. 6 shows this result even more clearly with the sample limited to stars with $T_{eff} > 5850$ K: GSE stars, and the retrograde halo stars, are confined to a small region of A_{Li}. The prograde halo and the disc sample show a larger range of A_{Li}, but if we look at only the stars with [Fe/H] < -1.3, these stars are constant A_{Li} with [Fe/H].

To quantify the Spite plateau A_{Li} abundance, we consider only stars with [Fe/H] < -1.3, because stars above this metallicity in the prograde halo and disc samples begin to show a divergence from the Spite plateau. This divergence is likely the signature of Galactic lithium evolution (Bensby & Lind 2018), and not self-depletion or self-enrichment of lithium in these stars. A bootstrap method was used to estimate the mean and standard deviation for each population. For each sample of stars, we resampled the A_{Li} values with replacement 1000 times. For each resampled set of values we found the mean and the standard deviation, and then found the mean and the standard deviation of these 1000 values. In the top row of Fig. 6 the coloured horizontal line is the mean of the 1000 mean values, and the shaded region indicates the average of the 1000 standard deviations.

For all 251 GALAH dwarf stars with $T_{eff} > 5850$ K, [Fe/H] < -1.3, and measured lithium abundance, we find the Spite plateau has a mean of $A_{Li} = 2.35 \pm 0.01$ and a spread of $\sigma_{A_{Li}} = 0.12 \pm 0.01$. For the four subsets of stars:

(i) 37 GSE stars: $A_{Li} = 2.37 \pm 0.02$, $\sigma_{A_{Li}} = 0.12 \pm 0.02$;
(ii) 45 retrograde halo stars: $A_{Li} = 2.37 \pm 0.02$, $\sigma_{A_{Li}} = 0.15 \pm 0.03$;
(iii) 34 prograde halo stars: $A_{Li} = 2.35 \pm 0.02$, $\sigma_{A_{Li}} = 0.10 \pm 0.01$;
(iv) 40 disc stars: $A_{Li} = 2.33 \pm 0.02$, $\sigma_{A_{Li}} = 0.14 \pm 0.02$.

The metallicity range for which GALAH provides reliable metallicities is [Fe/H] $> \sim -3$, and we confirm (as has previously been seen; e.g. Rebolo, Molaro & Beckman 1988; Meléndez et al. 2010) that the Spite plateau is basically flat with metallicity for stars within this metallicity regime. The four subsamples of stars show essentially identical mean A_{Li} abundances.

To summarize, we do not find any evidence to support the hypothesis that the formation environment affects the Spite plateau. This result is not overly surprising. While, it was previously difficult to identify stars in the Milky Way that truly formed in another galaxy, there was a consensus that a large fraction of the halo was accreted during the hierarchal mergers. So the prior literature on the Spite plateau (e.g. Pinsonneault et al. 1992, 1999; Ryan et al. 1999; Meléndez & Ramírez 2004; Bonifacio et al. 2007) will have certainly contained some mixture of *in situ* and *ex situ* stars. If there was some large difference in the formation lithium abundance of stars that was driven by their host galaxy, then this should have been obvious as a large scatter in the Spite plateau – something that is not seen at the metallicities considered in this work.

6 METAL-POOR STARS ABOVE THE SPITE PLATEAU

In Fig. 6, we have highlighted with purple squares those metal-poor stars in each population that show A_{Li} near or above the BBN lithium abundance. Most of these stars are found in the disc sample, and all of the Li-rich disc dwarfs are found on the warm peninsula (Fig. 6p). As discussed in Gao et al. (2020), metal-poor stars with these properties could be stars that have truly retained the BBN abundance.

For the halo and GSE samples, there are four metal-poor stars that sit well above the Spite plateau. Unlike the hot ($T_{eff} > 6500$ K) stars of the disc mentioned above, these stars are cooler and so should sit on the Spite plateau. Such Li-rich stars have been observed in globular clusters (Koch, Lind & Rich 2011; Monaco et al. 2012) and in the field (Bonifacio & Molaro 1997; Asplund et al. 2006). Within the framework for the Spite plateau proposed by Fu et al. (2015) – lithium depletion by the stars, followed by accretion from the interstellar medium – such lithium-rich stars could also be the result of an increase of the accretion process.

They could be the result of mass transfer from an asymptotic giant branch (AGB) companion. The GALAH `flag_sp` includes

Table 1. Stellar parameters and lithium abundances for those stars identified as belonging the Spite plateau in GALAH DR3. Here we show only the four stars from the GSE and retrograde halo samples that appear to be lithium enrichment (Fig. 6). The full table is available as supplementary material.

star_id	sobject_id	dr3_source_id	$T_{\rm eff}$	log g	[Fe/H]	$A_{\rm Li}$	Population
08295313+1621105	160110002601062	658743190301110144	5988	3.98	−1.43	2.72	GES
13433203−3940090	190223003301120	6113351720646486528	5956	3.84	−1.38	2.81	GES
03355522−6833454	131116000501386	4667364088963367808	5874	4.29	−1.33	3.02	Retrograde halo
15123917−1944545	170507008301377	6256414985329648384	6338	4.29	−1.94	2.70	Retrograde halo

bits to signify stars that could be binaries – either because they sit on the equal-mass binary sequence, or are found colocated with other binaries in the t-distributed stochastic neighbour embedding (t-SNE) projections. However, all the stars considered in this work have `flag_sp == 0`, so were not flagged as possible binaries. One of the stars does have a large $v_{\rm broad}$, indicating it has broad spectral lines – this could be a possible signature of binarity. If these stars were the product of mass transfer from an AGB companion, then this might manifest in the s-process abundances, which are shown for these stars in Fig. 7. Interpretation of neutron-capture element abundances in GALAH at low metallicity should be treated with caution as there is a strong metallicity-dependent detection limit. For the very lithium-rich retrograde halo star (blue square), it is clearly Ba and Y enhanced – though there are also several 'lithium-normal' stars of similar s-process abundances. Conversely, the most lithium-rich GSE star has low Ba and undetected Y.

Alternatively, it could represent lithium enrichment of the interstellar medium from which the stars formed. Models and observations of the Milky Way have its overall $A_{\rm Li}$ increasing at around [Fe/H] ~ -0.8 (Bensby & Lind 2018; Cescutti & Molaro 2019). This increase is driven by carbon–oxygen classical novae that produce ^{7}Be that then decays to ^{7}Li (Grisoni et al. 2019; Starrfield et al. 2020). Cescutti et al. (2020) and Molaro et al. (2020) both investigated evidence for lithium enrichment in GSE, with their models predicting the enrichment of lithium would occur at [Fe/H] ~ -1.2, a lower metallicity than in the Milky Way. Fig. 6 shows an exemplar Galactic lithium evolution model from Cescutti & Molaro (2019) as the solid black curve, and Fig. 6(a) also has a lithium enrichment model for GSE from Cescutti et al. (2020) as the dashed curve. These novae have similar progenitors (white dwarfs in binaries) as SNe Ia, Cescutti et al. (2020) assume a similar time delay of ∼1 Gyr before the onset of novae as typically assumed for SNe Ia. Thus an upturn in lithium abundance should occur at around the same time (i.e. [Fe/H]) as the downturn in [α/Fe]. We clearly see this downturn in [α/Fe] (Fig. 5c), but there is very much a lack of lithium-rich GES stars (Fig. 6a). There are only two GSE stars with enhanced lithium at lower metallicities, but they both at [Fe/H] < -1, lower than the metallicity predicted by Cescutti et al. (2020) for the Li enrichment. Both can be seen to have orbital actions consistent with GSE, and one definitely has a low α abundance, so there is nothing to rule out their GSE membership. GES is not the only accretion contributor to the halo of the Milky Way. So, there would be a variety of formation galaxy masses that have contributed. We might therefore expect to find many metal-poor stars above the Spite plateau, but there are just four in our sample of 251 stars.

7 SUMMARY

One of the main aims of Galactic archaeology, and in particular the GALAH survey, is to link the observations of the Milky Way to those of other galaxies – the concept of 'near-field cosmology' (Freeman & Bland-Hawthorn 2002). Within the Milky Way we have the ability to measure the properties and abundances of millions of individual stars to great precision, something that is only possible for some of the most luminous stars in nearby galaxies.

The *Gaia* revolution has shown the Milky Way contains a plethora of spatial and kinematic substructure (see the review by Helmi 2020), confirming the model of hierarchical galaxy formation. One of the dominant features is GSE, postulated to be the accretion remnant of a dwarf galaxy with a mass similar to the present-day Large Magellanic Cloud. It provides a large sample of identifiable *ex situ* formed stars, readily observable with moderate-sized telescopes. Every Galactic stellar survey with a simple selection that includes halo stars will have a large sample of GSE stars.

In this work, we have used results from GALAH DR3 to investigate the lithium abundance of ∼100 GSE stars. In particular we are interested in whether the formation environment of stars could be part of the solution to the cosmological lithium problem – the observed discrepancy between the primordial amount of lithium predicted to have been formed by BBN and the amount of lithium observed in warm, metal-poor stars (Fields 2011).

The large data set of GALAH makes it possible to carefully consider the effects of stellar parameters on the observed lithium abundance of stars (Section 3). The lithium abundance of a star cannot be considered in isolation from the observed stellar parameters, as standard models of stellar evolution do not successfully predict the observed trends between the lithium abundance of a star and its $T_{\rm eff}$, log g, and [Fe/H]. As shown in Fig. 2, there are features such as the lithium-dip region and the warm peninsula, which were studied in detail with the same data by Gao et al. (2020). For the purposes of studying the Spite plateau here we require stars to have $T_{\rm eff} > 5850$ K, because this is the region of parameter space that contains stars least affected by main-sequence lithium depletion.

To identify stars from the GSE we used orbital angular momenta and integrals of motion. Fig. 4 shows that GSE stars are found to have large J_R and $J_\phi \approx 0$ Mpc km s^{-1}. Kinematic substructure cannot be identified as accreted solely from its position in dynamical space. Jean-Baptiste et al. (2017) showed with high-resolution, dissipationless N-body simulations that in various dynamical parameter spaces there is considerable overlap between the *in situ* and the accreted populations. Figs 3 and 5 show that our GSE selection does appear to be relatively free from contamination by obvious *in situ* stars – the metallicity CDF is very similar for the prograde and retrograde populations of stars with $J_R > 30$ (kpc km s^{-1})$^{1/2}$; and our GSE stars with [Fe/H] > -1 show low α-element abundances as expected for stars that formed in a low galactic mass system.

The main conclusion of this work is that the formation environment of a warm, metal-poor halo star does not play a role in its main-sequence lithium abundance. There is no obvious difference in the lithium abundance, or its scatter, for metal-poor ($-3 <$ [Fe/H] < -1.3) stars from the GSE compared to stars from the halo or disc. In

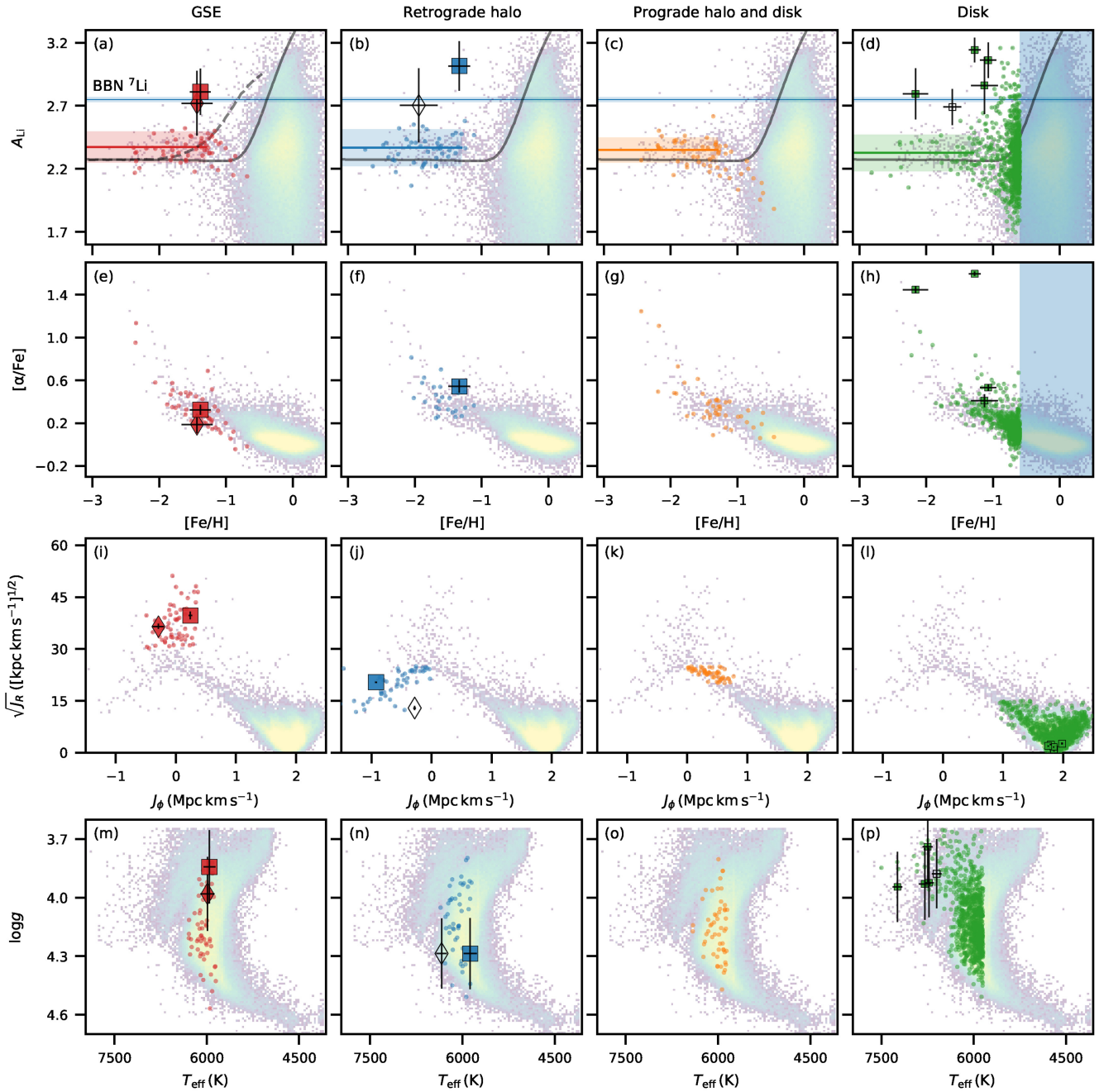

Figure 6. The (top row) $A_{\rm Li}$–[Fe/H], (second row) [α/Fe]–[Fe/H], J_ϕ–J_R (third row), and (bottom row) $T_{\rm eff}$–log g distributions for the four dynamically selected populations of stars – GSE (first column), retrograde halo (second column), prograde halo (third column), and disc (fourth column). The background distribution on all panels is all dwarf stars in GALAH with reliable lithium abundances. For each group the stars that meet the $T_{\rm eff}$–age criteria (Section 3 and Fig. 2) are highlighted. For visual clarity, the disc sample has been truncated to only show stars with [Fe/H] < -0.6. In the top row, the coloured horizontal line and shaded region indicate the average and standard deviation of stars with [Fe/H] < -1.3, i.e. the Spite plateau for that population. Highlighted with black-edged squares or diamond symbols (filled for stars with a reliable [α/Fe]; different symbols on the GSE and retrograde halo are simply to help the reader distinguish the two stars) are those stars from each group that have $A_{\rm Li} > 2.65$, i.e. they have lithium abundances near or above the BBN $A_{\rm Li}$ amount ($A_{\rm Li} = 2.75 \pm 0.02$; Pitrou et al. 2018). These stars are of interest for the accreted samples (GSE and the retrograde halo) as they could represent possible lithium enrichment in their formation environments. The solid black line is a thin disc evolutionary model from Cescutti & Molaro (2019), and the dashed black line is an evolutionary model for GSE from Cescutti et al. (2020).

particular, stars from the retrograde halo – which represent a stellar population that is likely to be either accreted or formed in the ancient proto-Galaxy – are indistinguishable from the GSE stars. This fits with the framework that sees the Spite plateau as the consequence of a lithium depletion by stars themselves.

This work used the motivation of the model proposed by Piau et al. (2006) that the Spite plateau is simply the result of the first generation of stars of a galaxy efficiently depleting lithium. We extended this to a more general idea that, like α-element abundances, different galaxies would leave a different imprint on the lithium abundances.

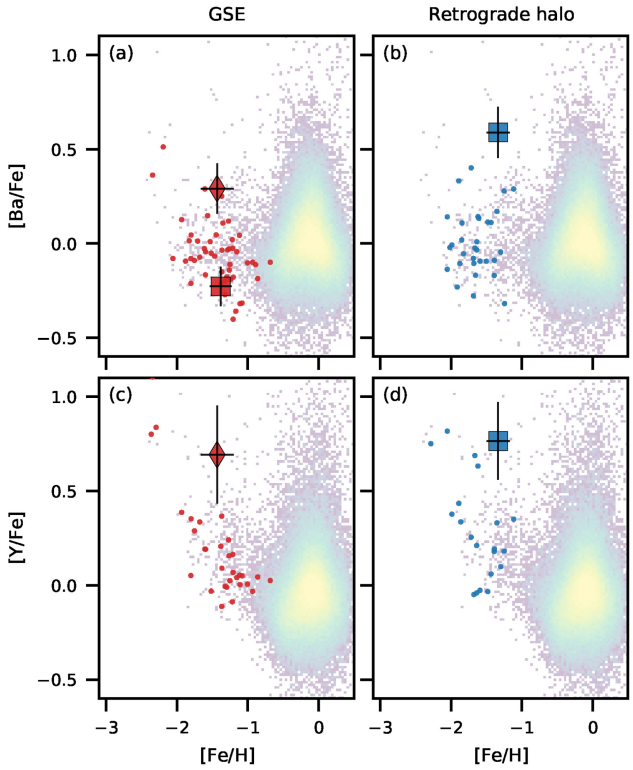

Figure 7. The s-process abundances of the lithium-rich halo dwarf stars found in GALAH. The symbols are the same as in Fig. 6. The lack of stars in the lower left-hand quadrant of the panels is related to detection limitations of HERMES spectra. There does not appear to be any correlation between lithium and s-process enrichment. Two of the stars with high Li abundances have high s-process abundances, but two have either normal-to-low or no measurable s-process abundances.

It should be noted that this proposed scenario has been rejected (e.g. Prantzos 2010, 2012) on the basis as it requires processing over two-thirds of all baryonic matter in very short-lived stars prior to any of the present-day halo stars formed, including at [Fe/H] < -3. Such massive star formation would produce large amounts of metals when exploding as super- and hypernovae and thus raise the metallicities to well above those of the halo stars.

The other notable result from that there are four stars in the halo or GSE with lithium abundances near or above the BBN value. A handful of such stars have been seen before (Bonifacio & Molaro 1997; Asplund et al. 2006; Koch et al. 2011; Monaco et al. 2012). It is possible that they are the consequence of post-formation accretion, from either a companion, or the interstellar medium from which they formed.

ACKNOWLEDGEMENTS

The GALAH survey is based on observations made at the Anglo-Australian Telescope, under programmes A/2013B/13, A/2014A/25, A/2015A/19, and A/2017A/18. We acknowledge the traditional owners of the land on which the AAT stands, the Gamilaraay people, and pay our respects to elders past, present, and emerging. This paper includes data that have been provided by AAO Data Central (datacentral.org.au).

The following software and programming languages made this research possible: PYTHON (v3.9.1); ASTROPY (v4.2; Astropy Collaboration et al. 2018), a community-developed core PYTHON package for astronomy; MATPLOTLIB (v3.3.3; Hunter 2007; Caswell et al. 2020); SCIPY (v1.6.0; Virtanen et al. 2020); and H5PY (v3.1.0).

This work has made use of data from the European Space Agency (ESA) mission *Gaia* (https://www.cosmos.esa.int/gaia), processed by the *Gaia* Data Processing and Analysis Consortium (DPAC, https://www.cosmos.esa.int/web/gaia/dpac/consortium). Funding for the DPAC has been provided by national institutions, in particular the institutions participating in the *Gaia* Multilateral Agreement.

Parts of this research were conducted by the Australian Research Council Centre of Excellence for All Sky Astrophysics in 3 Dimensions (ASTRO 3D), through project number CE170100013. JDS, SLM, and DBZ acknowledge the support of the Australian Research Council through Discovery Project grant DP180101791. SLM and JDS are supported by the UNSW Scientia Fellowship program. KL acknowledges funds from the European Research Council (ERC) under the European Union's Horizon 2020 Framework Programme (grant agreement no. 852977). Y-ST is grateful to be supported by the NASA Hubble Fellowship grant *HST*-HF2-51425.001 awarded by the Space Telescope Science Institute. ARC is supported in part by the Australian Research Council through a Discovery Early Career Researcher Award (DE190100656).

DATA AVAILABILITY

The data underlying this paper are available in the AAO Data Central.

The GALAH DR3 catalogue, several value-added catalogues, and all HERMES spectra of the sources are available for download via the Data Central service at datacentral.org.au. The accompanying documentation can be found at docs.datacentral.org.au/galah, and a full description of the data release is given in Buder et al. (2021).

REFERENCES

Abadi M. G., Navarro J. F., Fardal M., Babul A., Steinmetz M., 2010, MNRAS, 407, 435
Aguado D. S. et al., 2021, MNRAS, 500, 889
Alpher R. A., Bethe H., Gamow G., 1948, Phys. Rev., 73, 803
Asplund M., Lambert D. L., Nissen P. E., Primas F., Smith V. V., 2006, ApJ, 644, 229
Asplund M., Grevesse N., Sauval A. J., Scott P., 2009, ARA&A, 47, 481
Astropy Collaboration et al., 2018, AJ, 156, 123
Aver E., Olive K. A., Skillman E. D., 2015, J. Cosmol. Astropart. Phys., 07, 011
Bailyn C. D., 1995, ARA&A, 33, 133
Barbá R. H., Minniti D., Geisler D., Alonso-García J., Hempel M., Monachesi A., Arias J. I., Gómez F. A., 2019, ApJ, 870, L24
Belokurov V., Erkal D., Evans N. W., Koposov S. E., Deason A. J., 2018, MNRAS, 478, 611
Bensby T., Lind K., 2018, A&A, 615, A151
Bensby T., Oey M. S., Feltzing S., Gustafsson B., 2007, ApJ, 655, L89
Bland-Hawthorn J., Gerhard O., 2016, ARA&A, 54, 529
Boesgaard A. M., Lum M. G., Deliyannis C. P., King J. R., Pinsonneault M. H., Somers G., 2016, ApJ, 830, 49
Bonifacio P., Molaro P., 1997, MNRAS, 285, 847
Bonifacio P. et al., 2007, A&A, 462, 851
Borsato N. W., Martell S. L., Simpson J. D., 2020, MNRAS, 492, 1370
Bovy J., 2015, ApJS, 216, 29
Buder S. et al., 2018, MNRAS, 478, 4513
Buder S. et al., 2021, MNRAS, 506, 150
Casagrande L., 2020, ApJ, 896, 26
Casey A. R. et al., 2014, MNRAS, 443, 828
Caswell T. A. et al., 2020, matplotlib/matplotlib v3.1.3 (Version v3.1.3). Zenodo, Available at: http://doi.org/10.5281/zenodo.3633844
Cescutti G., Molaro P., 2019, MNRAS, 482, 4372

Cescutti G., Molaro P., Fu X., 2020, Mem. Soc. Astron. Ital., 91, 153
Charbonnel C., Talon S., 2005, EAS Publ. Ser., 17, 167
Cole S., Lacey C. G., Baugh C. M., Frenk C. S., 2002, MNRAS, 319, 168
Cooke R. J., Pettini M., Steidel C. C., 2018, ApJ, 855, 102
Cyburt R. H., Fields B. D., Olive K. A., Yeh T.-H., 2016, Rev. Mod. Phys., 88, 015004
Das P., Hawkins K., Jofré P., 2020, MNRAS, 493, 5195
Deliyannis C. P., Demarque P., Kawaler S. D., 1990, ApJS, 73, 21
De Silva G. M. et al., 2015, MNRAS, 449, 2604
Famaey B., Jorissen A., Luri X., Mayor M., Udry S., Dejonghe H., Turon C., 2005, A&A, 430, 165
Fattahi A. et al., 2019, MNRAS, 484, 4471
Feuillet D. K., Feltzing S., Sahlholdt C. L., Casagrande L., 2020, MNRAS, 497, 109
Fields B. D., 2011, Annu. Rev. Nucl. Part. Sci., 61, 47
Fields B. D., Olive K. A., Yeh T.-H., Young C., 2020, J. Cosmol. Astropart. Phys., 03, 010
Forbes D. A., Bridges T., 2010, MNRAS, 404, 1203
Freeman K., Bland-Hawthorn J., 2002, ARA&A, 40, 487
Fu X., Bressan A., Molaro P., Marigo P., 2015, MNRAS, 452, 3256
Gaia Collaboration et al., 2016, A&A, 595, A1
Gaia Collaboration et al., 2018, A&A, 616, A10
Gaia Collaboration et al., 2021, A&A, 649, A1
Gamow G., Landau L., 1933, Nature, 132, 567
Gao X. et al., 2020, MNRAS, 497, L30
Gratton R., 2020, in Bragaglia A., Davies M. B., Sills A., Vesperini E., eds, Proc. IAU Symp. Vol. 351, Star Clusters: From the Milky Way to the Early Universe. Cambridge Univ. Press, Cambridge, p. 241
Gravity Collaboration et al., 2019, A&A, 625, L10
Grisoni V., Matteucci F., Romano D., Fu X., 2019, MNRAS, 489, 3539
Haywood M., Di Matteo P., Lehnert M. D., Snaith O., Khoperskov S., Gómez A., 2018, ApJ, 863, 113
Helmi A., 2020, ARA&A, 58, 205
Helmi A., White S. D. M., de Zeeuw P. T., Zhao H., 1999, Nature, 402, 53
Helmi A., Babusiaux C., Koppelman H. H., Massari D., Veljanoski J., Brown A. G. A., 2018, Nature, 563, 85
Horta D. et al., 2020, MNRAS, 493, 3363
Howk J. C., Lehner N., Fields B. D., Mathews G. J., 2012, Nature, 489, 121
Hunter J. D., 2007, Comput. Sci. Eng., 9, 90
Ibata R. A., Gilmore G., Irwin M. J., 1994, Nature, 370, 194
Ibata R., Chapman S., Ferguson A. M. N., Irwin M., Lewis G., McConnachie A., 2004, MNRAS, 351, 117
Ibata R. A., Malhan K., Martin N. F., Starkenburg E., 2018, ApJ, 865, 85
Ibata R. A., Malhan K., Martin N. F., 2019, ApJ, 872, 152
Jean-Baptiste I., Di Matteo P., Haywood M., Gómez A., Montuori M., Combes F., Semelin B., 2017, A&A, 604, A106
Ji A. P. et al., 2020, AJ, 160, 181
Keller B. W., Kruijssen J. M. D., Pfeffer J., Reina-Campos M., Bastian N., Trujillo-Gomez S., Hughes M. E., Crain R. A., 2020, MNRAS, 495, 4248
Kobayashi C., Karakas A. I., Lugaro M., 2020, ApJ, 900, 179
Koch A., Lind K., Rich R. M., 2011, ApJ, 738, L29
Koppelman H., Helmi A., Veljanoski J., 2018, ApJ, 860, L11
Kos J. et al., 2017, MNRAS, 464, 1259
Lewis I. J. et al., 2002, MNRAS, 333, 279
Li C., Wang Y., Milone A. P., 2019, ApJ, 884, 17
Li C., Wang Y., Tang B., Milone A. P., Yang Y., Ji X., 2020, ApJ, 893, 17
McMillan P. J., 2017, MNRAS, 465, 76
Malhan K., Ibata R. A., Martin N. F., 2018, MNRAS, 481, 3442
Martell S. L. et al., 2017, MNRAS, 465, 3203
Massari D., Koppelman H. H., Helmi A., 2019, A&A, 630, L4
Mateu C., Read J. I., Kawata D., 2018, MNRAS, 474, 4112
Meléndez J., Ramírez I., 2004, ApJ, 615, L33
Meléndez J., Casagrande L., Ramírez I., Asplund M., Schuster W. J., 2010, A&A, 515, L3
Michaud G., Charbonneau P., 1991, Space Sci. Rev., 57, 1
Molaro P., Cescutti G., Fu X., 2020, MNRAS, 496, 2902
Monaco L., Villanova S., Bonifacio P., Caffau E., Geisler D., Marconi G., Momany Y., Ludwig H.-G., 2012, A&A, 539, A157
Monaco L., Villanova S., Carraro G., Mucciarelli A., Moni Bidin C., 2018, A&A, 616, A181
Monty S., Venn K. A., Lane J. M. M., Lokhorst D., Yong D., 2020, MNRAS, 497, 1236
Mucciarelli A., Salaris M., Bonifacio P., Monaco L., Villanova S., 2014, MNRAS, 444, 1812
Myeong G. C., Evans N. W., Belokurov V., Sanders J. L., Koposov S. E., 2018a, ApJ, 856, L26
Myeong G. C., Evans N. W., Belokurov V., Sanders J. L., Koposov S. E., 2018b, ApJ, 863, L28
Myeong G. C., Vasiliev E., Iorio G., Evans N. W., Belokurov V., 2019, MNRAS, 488, 1235
Naidu R. P., Conroy C., Bonaca A., Johnson B. D., Ting Y.-S., Caldwell N., Zaritsky D., Cargile P. A., 2020, ApJ, 901, 48
Nissen P. E., Schuster W. J., 2010, A&A, 511, L10
Nissen P. E., Schuster W. J., 2012, A&A, 543, A28
Oser L., Ostriker J. P., Naab T., Johansson P. H., Burkert A., 2010, ApJ, 725, 2312
Piau L., Beers T. C., Balsara D. S., Sivarani T., Truran J. W., Ferguson J. W., 2006, ApJ, 653, 300
Pinsonneault M. H., Deliyannis C. P., Demarque P., 1992, ApJS, 78, 179
Pinsonneault M. H., Walker T. P., Steigman G., Narayanan V. K., 1999, ApJ, 527, 180
Pitrou C., Coc A., Uzan J.-P., Vangioni E., 2018, Phys. Rep., 754, 1
Prantzos N., 2010, PoS, NIC-IX, 254
Prantzos N., 2012, A&A, 542, A67
Randich S., Magrini L., 2021, Frontiers Astron. Space Sci., 8, 616201
Rebolo R., Molaro P., Beckman J. E., 1988, A&A, 192, 192
Reid M. J., Brunthaler A., 2004, ApJ, 616, 872
Richard O., 2012, Mem. Soc. Astron. Ital. Suppl., 22, 211
Ryan S. G., Norris J. E., Beers T. C., 1999, ApJ, 523, 654
Salpeter E. E., 1955, Phys. Rev., 97, 1237
Sbordone L. et al., 2010, A&A, 522, A26
Schönrich R., Binney J., Dehnen W., 2010, MNRAS, 403, 1829
Searle L., Zinn R., 1978, ApJ, 225, 357
Sharma S. et al., 2018, MNRAS, 473, 2004
Sharma S. et al., 2019, MNRAS, 490, 5335
Sheinis A. et al., 2015, J. Astron. Telesc. Instrum. Syst., 1, 035002
Simpson J. D. et al., 2020, MNRAS, 491, 3374
Spite F., Spite M., 1982a, A&A, 115, 357
Spite M., Spite F., 1982b, Nature, 297, 483
Starkenburg E., Oman K. A., Navarro J. F., Crain R. A., Fattahi A., Frenk C. S., Sawala T., Schaye J., 2017, MNRAS, 465, 2212
Starrfield S., Bose M., Iliadis C., Hix W. R., Woodward C. E., Wagner R. M., 2020, ApJ, 895, 70
Venn K. A., Irwin M., Shetrone M. D., Tout C. A., Hill V., Tolstoy E., 2004, AJ, 128, 1177
Virtanen P. et al., 2020, Nat. Methods, 17, 261
Wallerstein G., Herbig G. H., Conti P. S., 1965, ApJ, 141, 610
White S. D. M., Frenk C. S., 1991, ApJ, 379, 52
Williams M. E. K. et al., 2011, ApJ, 728, 102
Wittenmyer R. A. et al., 2018, AJ, 155, 84
Yan H.-L. et al., 2018, Nat. Astron., 2, 790
Yuan Z. et al., 2020, ApJ, 891, 39

SUPPORTING INFORMATION

Supplementary data are available at *MNRAS* online.

Table 1. Stellar parameters and lithium abundances for those stars identified as belonging the Spite plateau in GALAH DR3.

Please note: Oxford University Press is not responsible for the content or functionality of any supporting materials supplied by the authors.

Any queries (other than missing material) should be directed to the corresponding author for the article.

[1]*School of Physics, UNSW, Sydney, NSW 2052, Australia*
[2]*Centre of Excellence for Astrophysics in Three Dimensions (ASTRO-3D), Australia*
[3]*Research School of Astronomy and Astrophysics, Australian National University, ACT 2611, Canberra, Australia*
[4]*Sydney Institute for Astronomy, School of Physics (A28), The University of Sydney, Sydney, NSW 2006, Australia*
[5]*School of Physics and Astronomy, Monash University, Clayton, VIC 3800, Australia*
[6]*Australian Astronomical Optics, Faculty of Science and Engineering, Macquarie University, Macquarie Park, NSW 2113, Australia*
[7]*Macquarie University Research Centre for Astronomy, Astrophysics & Astrophotonics, Sydney, NSW 2109, Australia*
[8]*Istituto Nazionale di Astrofisica, Osservatorio Astronomico di Padova, vicolo dell'Osservatorio 5, I-35122 Padova, Italy*
[9]*Faculty of Mathematics and Physics, University of Ljubljana, Jadranska 19, 1000 Ljubljana, Slovenia*
[10]*Department of Astronomy, Stockholm University, AlbaNova University Centre, SE-106 91 Stockholm, Sweden*
[11]*Department of Physics and Astronomy, Macquarie University, Sydney, NSW 2109, Australia*
[12]*Max Planck Institute for Astrophysics, Karl-Schwarzschild-Str 1, D-85741 Garching, Germany*
[13]*Centre for Integrated Sustainability Analysis, The University of Sydney, Australia*
[14]*Centre for Astrophysics, University of Southern Queensland, Toowoomba, QLD 4350, Australia*
[15]*Institute for Advanced Study, Princeton, NJ 08540, USA*
[16]*Department of Astrophysical Sciences, Princeton University, Princeton, NJ 08544, USA*
[17]*Observatories of the Carnegie Institution of Washington, 813 Santa Barbara Street, Pasadena, CA 91101, USA*
[18]*Department of Physics and Astronomy, Johns Hopkins University, Baltimore, MD 21218, USA*

This paper has been typeset from a TEX/LATEX file prepared by the author.